

Draft writing

ENERGY AND MOMENTUM TRANSFER VIA COULOMB FRICTIONS IN RELATIVISTIC TWO FLUIDS

K. ASANO

Division of Theoretical Astronomy, National Astronomical Observatory of Japan

asano@th.nao.ac.jp

and

S. IWAMOTO

Software Cradle Co. Ltd.

and

F. TAKAHARA

Department of Earth and Space Science, Graduate School of Science, Osaka University

takahara@vega.ess.sci.osaka-u.ac.jp

Submitted; accepted

ABSTRACT

We numerically calculate the energy and momentum transfer rates due to Coulomb scattering between two fluids moving with a relative velocity. The results are fitted by simple functions. The fitting formulae are useful to simulate outflows from active galactic nuclei and compact high energy sources.

Subject headings: Relativistic thermal plasma

1. INTRODUCTION

Relativistic jets are observed in active galactic nuclei (AGN) and Galactic black hole candidates. The velocity of these jets are highly relativistic with a bulk Lorentz factor above 10. The kinetic power is almost comparable to the Eddington luminosity. The production and bulk acceleration of these jets are still unknown, though many ideas have been proposed ranging from magneto-hydrodynamical to radiative and thermal ones. There is no consensus on how jets are produced and accelerated.

Although it is difficult to determine the matter content of jets from observations, several independent arguments favor electron-positron jets (Takahara 1994, 1997; Reynolds et al. 1996; Wardle et al. 1998; Homan & Wardle 1999; Hirotani et al. 1999, 2000; Hirotani 2005; Kino & Takahara 2004; Croston et al. 2005). Electron-positron jets are most likely produced in accretion disks around the central black holes. Because the electron mass is much smaller than the proton mass, the produced electron-positron pairs can be ejected more easily than protons. Some papers discuss the accretion disks with electron-positron outflows (Misra & Melia 1995; Liang & Li 1995; Li & Liang 1996; Yamasaki et al. 1999). If the accretion disks form hot pair plasma strongly coupled with photons, the plasma may be thermally accelerated like the fireball applied to gamma-ray bursts. Iwamoto & Takahara (2002, 2004) showed that a “Wien fireball”, which is optically thick to Compton scattering but thin to absorption, results in a relativistic outflow avoiding the difficulties of pair annihilation and radiation drag.

Pairs are formed via photon-photon collisions in the accretion disk composed of normal plasma (electron-proton). Such pairs may escape from the disk by their own pressure or radiative force (Yamasaki et al. 1999). In order to investigate pair ejection from the disk, one needs to treat multi-component plasma dynamics with radiation field. However, there has been no study of formation and ejection of pairs from the accretion disk taking into account radiative transfer consistently. Such studies require knowledge of friction force between the background plasma and pair outflow. Although several plasma effects may be important, Coulomb scattering is the first one to be taken into account. The purpose of this paper is to obtain useful formulae of the energy and momentum transfers between two fluids moving with a relative velocity via Coulomb interaction.

The heating and cooling rates of thermal plasmas are well known in both non-relativistic (Spitzer 1956) and relativistic cases (Stepney 1983). Dermer (1985) analytically derived the energy exchange rate of two isotropic plasmas interacting at different temperatures. If there exists a relative velocity between two plasmas, analytical expressions of the energy and momentum exchange rates are hard to be obtained.

In this paper, we numerically obtain the energy and momentum exchange rates due to Coulomb scattering between two Maxwell-Boltzmann plasmas with a relative velocity. In another paper, we simulate pair outflows from hot plasmas (Asano & Takahara 2006) using the results in this paper. In §2 we describe a formulation of the reaction rates between two plasmas. In §3 we show the numerical results for parameter regions we are interested in. Fitting formulae are presented so that one can use our results in a numerical simulation of two fluid dynamics.

2. TWO-FLUIDS INTERACTION

In this section we describe a formulation of the exchange rates of energy and momentum due to Coulomb scattering in two fluids. Consider a collision of two particles, which belong to the fluids A and B, respectively. Before the collision their 4-momenta in the laboratory frame are

$$p_A^\mu = m_A c \gamma_A (1, \boldsymbol{\beta}_A), \quad p_B^\mu = m_B c \gamma_B (1, \boldsymbol{\beta}_B). \quad (1)$$

Here, m_i and $\boldsymbol{\beta}_i$ are the mass and velocity normalized by the light speed c of the particle in the fluid i , respectively. The Lorentz factor of the particle is denoted as $\gamma_i = (1 - \beta_i^2)^{-1/2}$, and that of the relative velocity β_r is written as

$$\gamma_r = \gamma_A \gamma_B (1 - \boldsymbol{\beta}_A \cdot \boldsymbol{\beta}_B), \quad (2)$$

which is Lorentz invariant.

The velocity of the center-of-mass (CM) in the laboratory frame is

$$\boldsymbol{\beta}_{\text{CM}} = \frac{m_A \gamma_A \boldsymbol{\beta}_A + m_B \gamma_B \boldsymbol{\beta}_B}{m_A \gamma_A + m_B \gamma_B}. \quad (3)$$

Let this direction define the x -axis in the Cartesian coordinate (x, y, z) in the laboratory frame, $\boldsymbol{\beta}_{\text{CM}} = \beta_{\text{CM}} \hat{x}$. The velocity of particles in the fluid i is decomposed as

$$\boldsymbol{\beta}_i = \beta_{ix} \hat{x} + \beta_{iy} \hat{y} + \beta_{iz} \hat{z}, \quad (4)$$

Denoting the 4-momentum of particles in the fluid A after the collision as $p_{A2}^\mu = m_A c \gamma_{A2} (1, \boldsymbol{\beta}_{A2})$, the exchange of 4-momentum is written as

$$\Delta p_A^\mu = m_A c (\gamma_{A2} - \gamma_A, \gamma_{A2} \boldsymbol{\beta}_{A2} - \gamma_A \boldsymbol{\beta}_A). \quad (5)$$

The mean exchange of energy for elastic scattering in the laboratory frame is

$$\langle \Delta E \rangle = \langle \Delta p_A^0 \rangle c = -\langle \Delta p_B^0 \rangle c$$

$$\begin{aligned}
&= 2m_A c^2 \gamma_A \gamma_{\text{CM}}^2 \sin^2(\alpha/2) \beta_{\text{CM}} (\beta_{\text{CM}} - \beta_{Ax}) \\
&= \frac{-2m_A m_B \sin^2(\alpha/2)}{m_A^2 + m_B^2 + 2\gamma_r m_A m_B} c^2 \\
&\quad \times [m_B \gamma_A - m_A \gamma_B + \gamma_r (m_A \gamma_A - m_B \gamma_B)].
\end{aligned} \tag{6}$$

(Stepney 1983), where α is the scattering angle in the CM-frame and $\gamma_{\text{CM}} = (1 - \beta_{\text{CM}}^2)^{-1/2}$. The mean momentum exchange in the laboratory frame is described as

$$\begin{aligned}
\langle \Delta p_A^x \rangle &= 2m_A c \gamma_A \gamma_{\text{CM}}^2 (\beta_{\text{CM}} - \beta_{Ax}) \sin^2(\alpha/2) \\
\langle \Delta p_A^y \rangle &= -2m_A c \gamma_A \beta_{Ay} \sin^2(\alpha/2) \\
\langle \Delta p_A^z \rangle &= -2m_A c \gamma_A \beta_{Az} \sin^2(\alpha/2)
\end{aligned} \tag{7}$$

Hereafter we denote the distribution functions of the fluid i as $n_i f_i(\mathbf{p}_i)$, where n_i is the number density of the fluid in the laboratory frame so that $\int f_i(\mathbf{p}_i) d^3 p_i = 1$. The scattering rate per unit volume,

$$R_{AB} = n_A f_A(\mathbf{p}_A) n_B f_B(\mathbf{p}_B) c \frac{\gamma_r \beta_r}{\gamma_A \gamma_B} \frac{d\sigma(\mathbf{p}_A, \mathbf{p}_B)}{d\Omega} d\Omega, \tag{8}$$

(Weaver 1976; Landau & Lifshitz 1975), is Lorentz-invariant. In this expression $d\Omega \equiv 2\pi \sin \alpha d\alpha$ and $d\sigma/d\Omega$ is the differential cross-section. The exchange rate of 4-momentum per unit volume dV and per unit time dt is described as

$$\frac{dP^\mu}{dt dV} = \frac{1}{1 + \delta_{AB}} \int \int \langle \Delta p^\mu \rangle R_{AB} d^3 p_A d^3 p_B, \tag{9}$$

Then, we now restrict the situation that particles in the fluid A have an isotropic Maxwell-Boltzmann (MB) distribution in the laboratory frame K and that particles in the fluid B have another isotropic MB distribution in another inertial frame K' . The relative velocity between the two frames is defined as β_R and its Lorentz factor is $\Gamma_R = (1 - \beta_R^2)^{-1/2}$.

The relativistic MB distribution of the fluid A in the laboratory frame is described as

$$f_A(\mathbf{p}_A) d^3 p_A = \frac{\exp(-\gamma_A/\theta_A)}{4\pi\theta_A K_2(1/\theta_A)} u_A^2 du_A d\Omega_A, \tag{10}$$

where $u_i = \gamma_i \beta_i$, $\theta_i \equiv T_i/m_i c^2$ is the temperature normalized by the mass of the particles, K_2 is the modified Bessel function of the 2nd kind, $d\Omega_i \equiv d\mu_i d\phi_i$ is the solid angle of \mathbf{p}_i , respectively. Because of Lorentz invariance of the distribution function, $n_B f_B = n'_B f'_B = n'_B \exp(-\gamma'_B/\theta_B)/(4\pi\theta_B K_2(1/\theta_B))$, where primed values represent quantities in the frame K' . Since $n'_B = n_B/\Gamma_R$, we obtain

$$f_B(\mathbf{p}_B) d^3 p_B = \frac{\exp(-\gamma'_B/\theta_B)}{4\pi\Gamma_R \theta_B K_2(1/\theta_B)} u_B^2 du_B d\Omega_B, \tag{11}$$

where $\gamma'_B = \Gamma_R(\gamma_B - \beta_R \mu_B u_B)$.

When the particle species in the fluids A and B are the same, we cannot determine if the scattered particle belongs to fluid A or B by the quantum mechanics principle. In this case, we treat as follows. As is well known, plasma relaxation is achieved by mainly small angle scattering ($\alpha \ll 1$). Therefore, it may be natural to consider that $\alpha \leq \pi/2$ in this case. Even if we allow large angle scattering ($\alpha > \pi/2$), we ought to consider that it means exchange of particles between the fluids A and B. As a result, we can use the above formulation assuming $\alpha \leq \pi/2$ for scatterings of the same species of particles.

The integral over α is analytically possible (see Appendix). On the other hand, from the axial symmetry the sextuple integral in equation (9) is reduced to a quintuple integral. However, further reduction in the order of integral may not be carried out differently from isotropic cases such as in Dermer (1985). Therefore, a straightforward method in numerical integration is inefficient in this case. Using a Monte Carlo technique that is similar to the method in Ramaty & Mészáros (1981), we numerically integrate equation (9) with $N = 10^9$ collisions of two particles whose momentum distributions are proportional to equations (10) and (11), respectively. The differential cross-sections we used are summarized in Appendix. The Coulomb logarithm $\ln \Lambda = 20$ is adopted throughout this paper.

3. NUMERICAL RESULTS

We calculate energy and momentum transfers (ET and MT) for probable temperatures of leptons and protons in hot accretion disks. The relative velocity of two fluids, $U_R = \sqrt{\Gamma_R^2 - 1}$, is in the range of $10^{-2} \leq U_R \leq 10^2$ in our calculation. Because of the property of the Monte Carlo method, estimated values of ET and MT may have errors especially for MT with $U_R \ll 1$. However, from our experiences, the errors are at most 10 % for $u_R > 0.1$. In contrast to the uncertainty in the Coulomb logarithm, these errors may be negligible.

We express the energy gain rate of the outflowing plasma (fluid B) as

$$\frac{dE}{dt dV} = n_A n_B m_e c^2 F_E(T_A, T_B, U_R). \quad (12)$$

in the laboratory frame (the comoving frame of the fluid A). The value F_E has a dimension of $[\text{cm}^3/\text{s}]$. We should notice that n_A and $n_B = \Gamma_R n'_B$ are densities in the laboratory frame.

On the other hand, the momentum loss rate of the outflowing plasma is expressed as

$$\frac{dP}{dt dV} = n_A n_B m_e c F_P(T_A, T_B, U_R). \quad (13)$$

The dimension of F_P is the same as that of F_E .

Since $dt dV$ is Lorentz invariant, these rates in the laboratory frame correlate with the rates in the comoving frame of the fluid B as

$$\frac{dE}{dt dV} = \Gamma_R \frac{dE'}{dt' dV'} - c U_R \frac{dP'}{dt' dV'} \quad (14)$$

$$\frac{dP}{dt dV} = \Gamma_R \frac{dP'}{dt' dV'} - \frac{U_R}{c} \frac{dE'}{dt' dV'}, \quad (15)$$

respectively, where the minus signs in the second terms are due to the definition of $dP/dt dV$ (momentum “loss” rate). The above equations show that negative energy gain rate ($dE/dt dV < 0$) does not necessarily imply a temperature drop of the fluid B. If the fluid B is decelerated rapidly ($dE'/dt' dV' \ll cdP'/dt' dV'$), the energy gain rate in the laboratory frame can be negative.

3.1. ENERGY TRANSFER in p-e INTERACTION

In this subsection we show the numerical results of ET between the background protons (A=p) and outflowing electrons or positrons (B=e). We assume the temperature of protons is higher than that of the electrons (positrons). Hereafter we denote the temperature of protons normalized by electron mass as $\Theta_p \equiv T_p/m_e c^2 = (m_p/m_e)\theta_p$. In Figure 1 we plot F_E for $\Theta_p = 10$. If $U_R = 0$, the energy gain rate is analytically obtained as

$$F_E(T_p, T_e, 0) = \frac{3\sigma_T}{2m_p c} \frac{T_p - T_e}{K_2(1/\theta_e)K_2(1/\theta_p)} \ln \Lambda \times \left[\frac{2(\theta_e + \theta_p)^2 + 1}{\theta_e + \theta_p} K_1\left(\frac{\theta_e + \theta_p}{\theta_e \theta_p}\right) + 2K_0\left(\frac{\theta_e + \theta_p}{\theta_e \theta_p}\right) \right], \quad (16)$$

(Stepney & Guilbert 1983). Our numerical results for $U_R \ll 1$ agree with the above analytical estimate. For $U_R \gtrsim 1.0$, F_E declines with U_R . If U_R is substantially larger than θ_e , we can neglect the thermal motion of leptons and F_E becomes independent of θ_e . Therefore, F_E agree with each other for $U_R \gg \theta_e$.

Unfortunately, we could not fit our results by a simple analytical function of Θ_p , θ_e , and U_R . In Figure 2 we plot F_E for $\Theta_p = 10^{0.75}$ as well as fitting functions. We fit the numerical results by two functions of U_R ; exponentially damped one for lower U_R , and power-law one for higher U_R as

$$F_E = \begin{cases} A_L \exp\left[-\left(\frac{U_R}{U_0}\right)^p\right], & \text{for } U_R < U_{\text{th}} \\ A_H U_R^r, & \text{for } U_R \geq U_{\text{th}}. \end{cases} \quad (17)$$

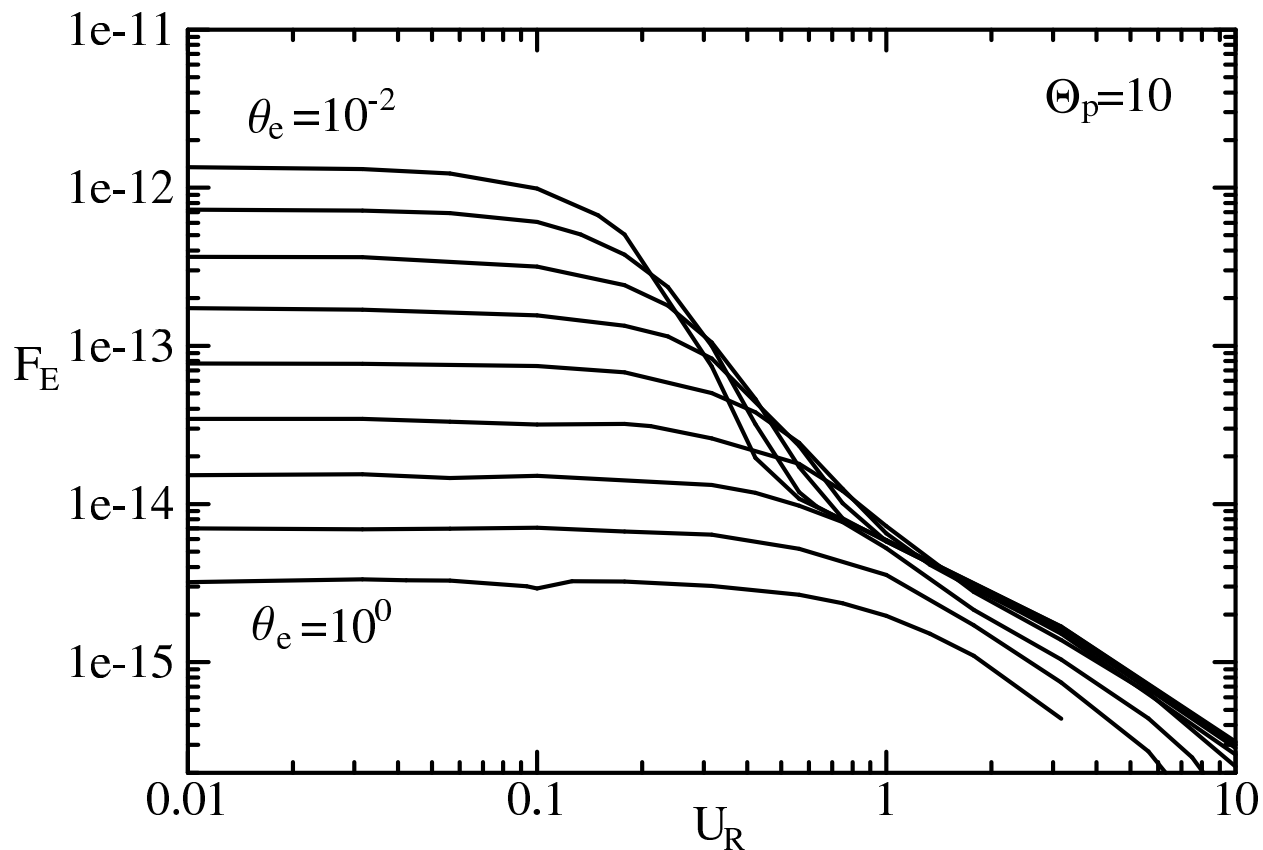


Fig. 1.— F_E of p-e interaction for $\Theta_p = 10.0$ in cgs unit. The temperatures of electrons (positrons), θ_e , are from 10^{-2} to 10^0 at $10^{0.25}$ intervals in logarithmic scale.

The energy gain rate of leptons F_E generally decreases with U_R and for $U_R \gg \Theta_p$ it becomes negative [see eq. (6)]. This corresponds to the deceleration of the lepton beam moving through cold medium. Since $U_R \ll m_p/m_e$ in our case, $\beta_{\text{CM}} \ll 1$, namely the CM frame is almost the same as the laboratory frame. For $U_R \gg \Theta_p$, the Lorentz factor of electrons in the CM frame γ (see APPENDIX) is approximated as $\sim \gamma_e \sim U_R \sim \gamma_r$. The equation (6) indicates the energy loss of electrons in one collision $\langle \Delta E \rangle \sim (m_e/m_p)U_R^2 m_e c^2 \sin^2(\alpha/2)$, while the effective cross-section (see APPENDIX) $\sigma_{\text{eff}} \propto \gamma^{-2} \propto U_R^{-2}$. Therefore, F_E (roughly proportional to $c\sigma_{\text{eff}}\langle \Delta E \rangle$) becomes negative and constant for $U_R \gg \Theta_p$ as shown in Figure 2.

Even for positive F_E the fitting functions (17) deviate for $U_R \sim \Theta_p$ as shown in Figure 2. However, the fitting formulae may be practically correct for $U_R \lesssim \Theta_p$. The fitting parameters A_L , p , U_0 , A_H , r , and U_{th} are listed in Tables 1-5. The parameter p is fixed as 2 except for Tables 1 and 5. We listed only for $\Theta_p = 10^{0.75}$, 10^1 , $10^{1.5}$, 10^2 , and $10^{2.5}$. One can interpolate

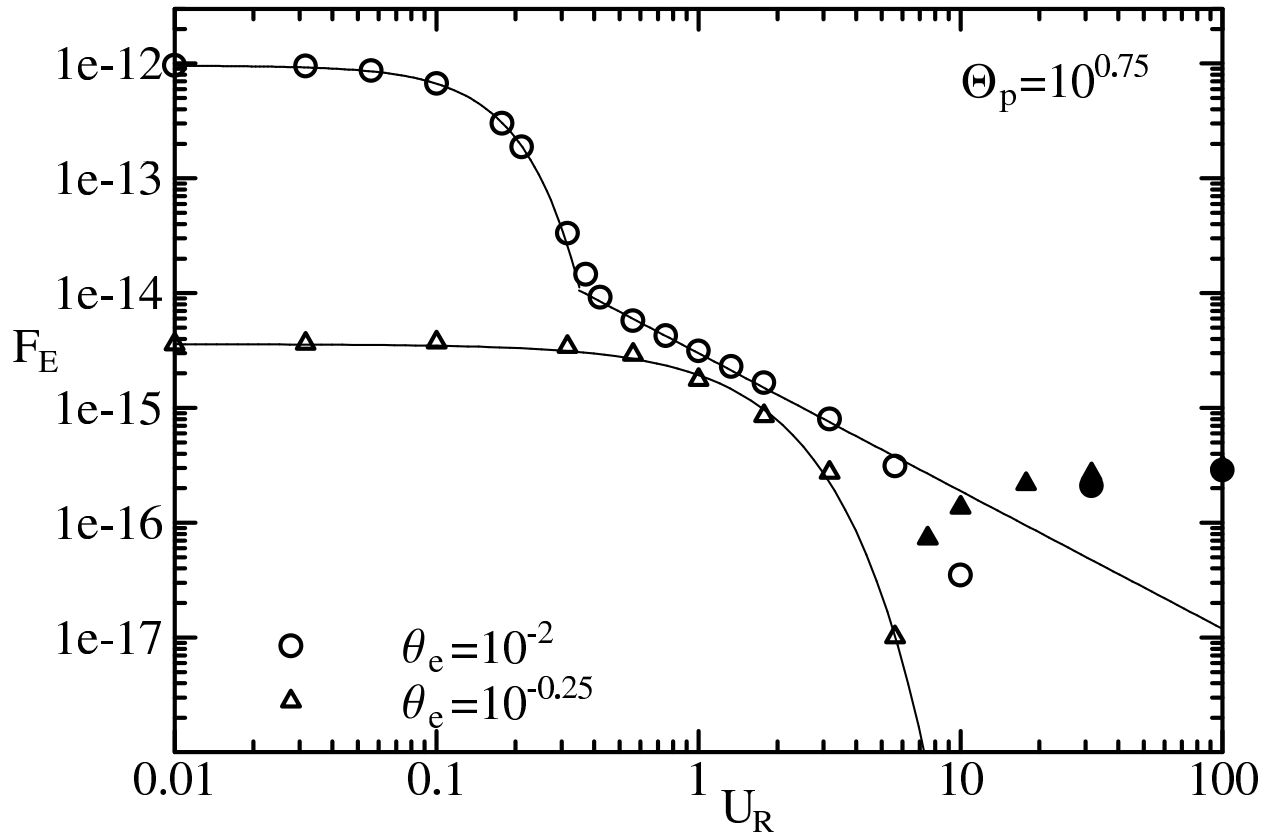


Fig. 2.— Two examples of the fitting functions for F_E of p-e interaction. Circles and triangles are numerical results. Filled symbols are $|F_E|$ for negative F_E . Solid lines are the fitting functions we obtained (see equation (17) and Table 1).

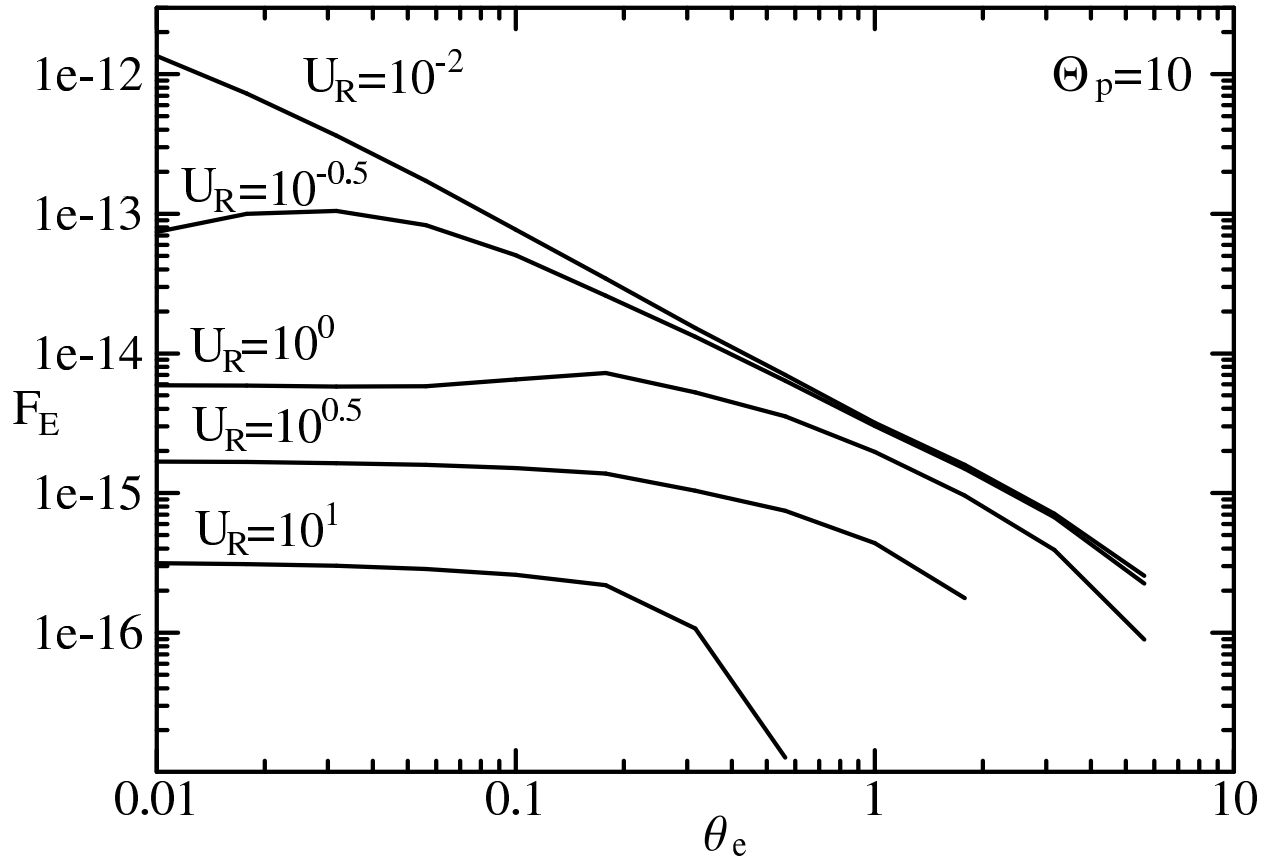


Fig. 3.— Same as Fig.1 but plotted vs. θ_e .

F_E for general values of Θ_p from our fitting formulae. Our fitting formulae give a satisfactory fit to numerical results for these ranges of Θ_p and U_R .

Although the numerical results smoothly change with θ_e as shown in Figure 1, the fitting parameters do not necessarily change monotonically. There exist numerical uncertainties of $\sim 10\%$ and the fitting method is not unique. For example, if we refit the results with a slight change of the “connecting point” U_{th} , the other parameters, especially indices p , q (see next subsection), and r , will change substantially. Therefore, as will be shown throughout this paper, parameter values we obtained do not always change systematically with θ_e .

In Figure 3 we plot F_E for $\Theta_p = 10$ as functions of θ_e for reference. The results are not necessarily monotonically decreasing functions of θ_e , while curves in Figure 1 decrease with increasing U_R .

3.2. MOMENTUM TRANSFER in p-e INTERACTION

The numerical results of F_P for $\Theta_p = 10$ are plotted in Figure 4. The value of F_P increases with increasing U_R for $U_R \ll 1$. At $U_R \sim 1$ F_P starts to decrease because of smallness of the cross sections in relativistic collisions. The results are fitted in the same way as F_E . The fitting formulae are written as

$$F_P = \begin{cases} A_L \exp\left[-\left(\frac{U_R}{U_0}\right)^p\right] \left(\frac{U_R}{0.01}\right)^q, & \text{for } U_R < U_{th}, \\ A_H U_R^r, & \text{for } U_R \geq U_{th}, \end{cases} \quad (18)$$

and the parameters are listed in Tables 6-10. As shown in Figure 5 the results are fitted by these functions within $\sim 10\%$ errors for a wide range of U_R .

Though a sufficient amount of momentum is exchanged for each collision of particles, the total momentum exchange between the two fluids is almost cancelled out for $U_R \ll \theta_e$. Since F_P comes from the bulk motion of the outflowing electrons, the behaviour, $F_P \propto U_R$ for $U_R \ll 1$, is a natural consequence. On the other hand, F_P decreases with U_R for $U_R \gtrsim 1$. From equations (6) and (7), the momentum loss of electrons $\langle \Delta p \rangle \sim \langle \Delta E \rangle / (c\beta_{CM})$ for $U_R \gg \Theta_p$. As discussed in §3.1, $\langle \Delta E \rangle \propto U_R^2$ and $\beta_{CM} \propto U_R$ in this case. Then, we obtain $F_P \propto U_R^{-1}$, which is consistent with the index r in the Tables.

In Figure 6 we plot F_P for $\Theta_p = 10$ as functions of θ_e for reference. The line for $U_R = 10^{-2}$ is not smooth probably owing to a statistical error in the Monte Carlo integral. Although the rate of momentum transfer is monotonically decreasing functions of θ_e , the behavior beyond and below $U_R \sim 1$ is apparently different. There exists a maximum value of F_P at $U_R \sim 1$ and the Coulomb friction becomes small as θ_e increases, because of the

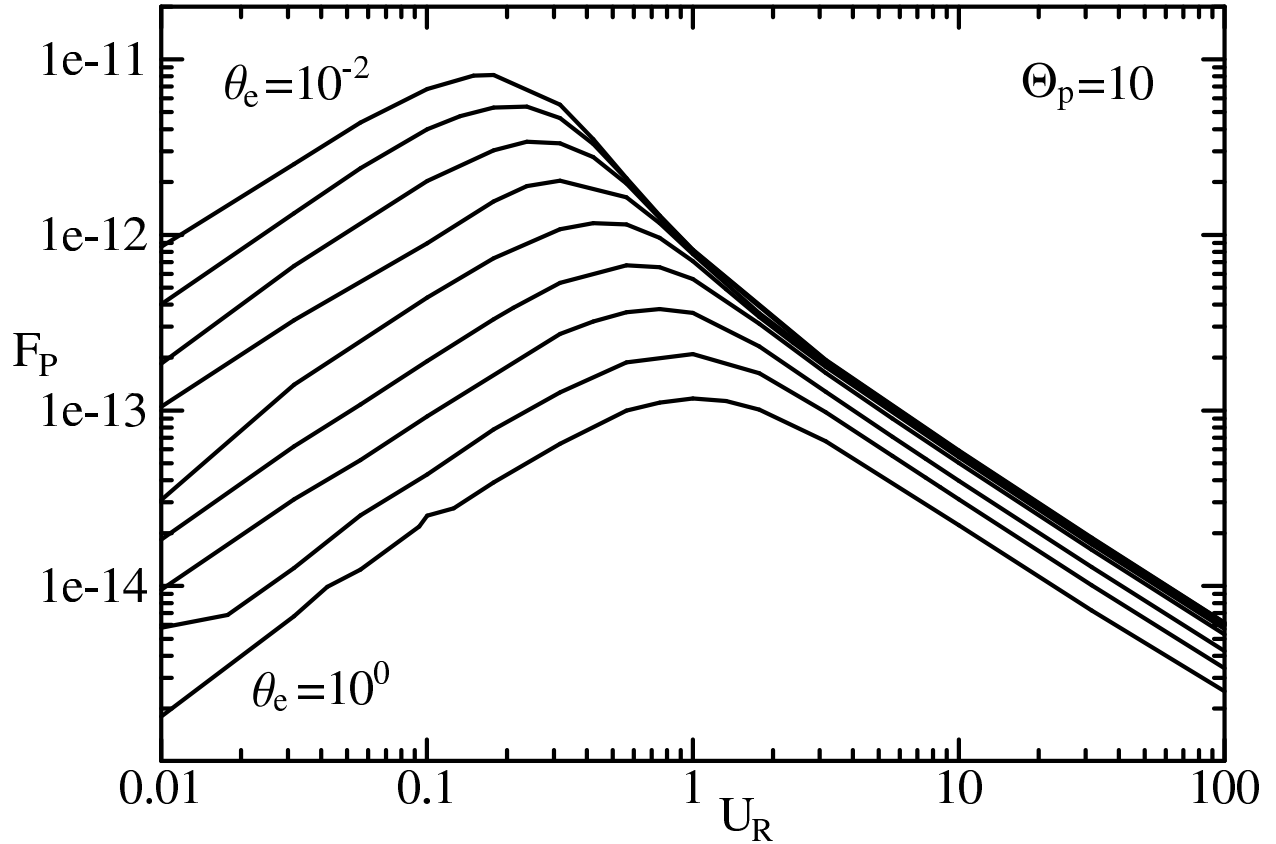


Fig. 4.— F_P of p-e interaction for $\Theta_p = 10.0$ in cgs unit. The temperatures of electrons (positrons) are same as those in Fig. 1.

monotonic behaviour of the cross section, $\sigma_{\text{eff}} \propto \gamma^{-2}\beta^{-4}$ (see APPENDIX).

3.3. ENERGY TRANSFER in e-e INTERACTION

In this subsection we show the results for ET between the background electrons ($A=be$) and outflowing electrons ($B=-$) or positrons ($B=+$). We assume that the temperature of the outflowing leptons is lower than the background electrons. In the opposite cases ET and MT are obtained from the Lorentz transformation of our results. The values for e^-e^- and e^-e^+ interactions are almost the same. Therefore, we only show the results for e^-e^- hereafter.

Figure 7 shows ET between two electron fluids for $\theta_{be} = 1$. For $\theta_- \lesssim 0.1$ the functional shapes of ET are almost invariant, because we can neglect the bulk motion for $U_R \ll \theta_{be}$.

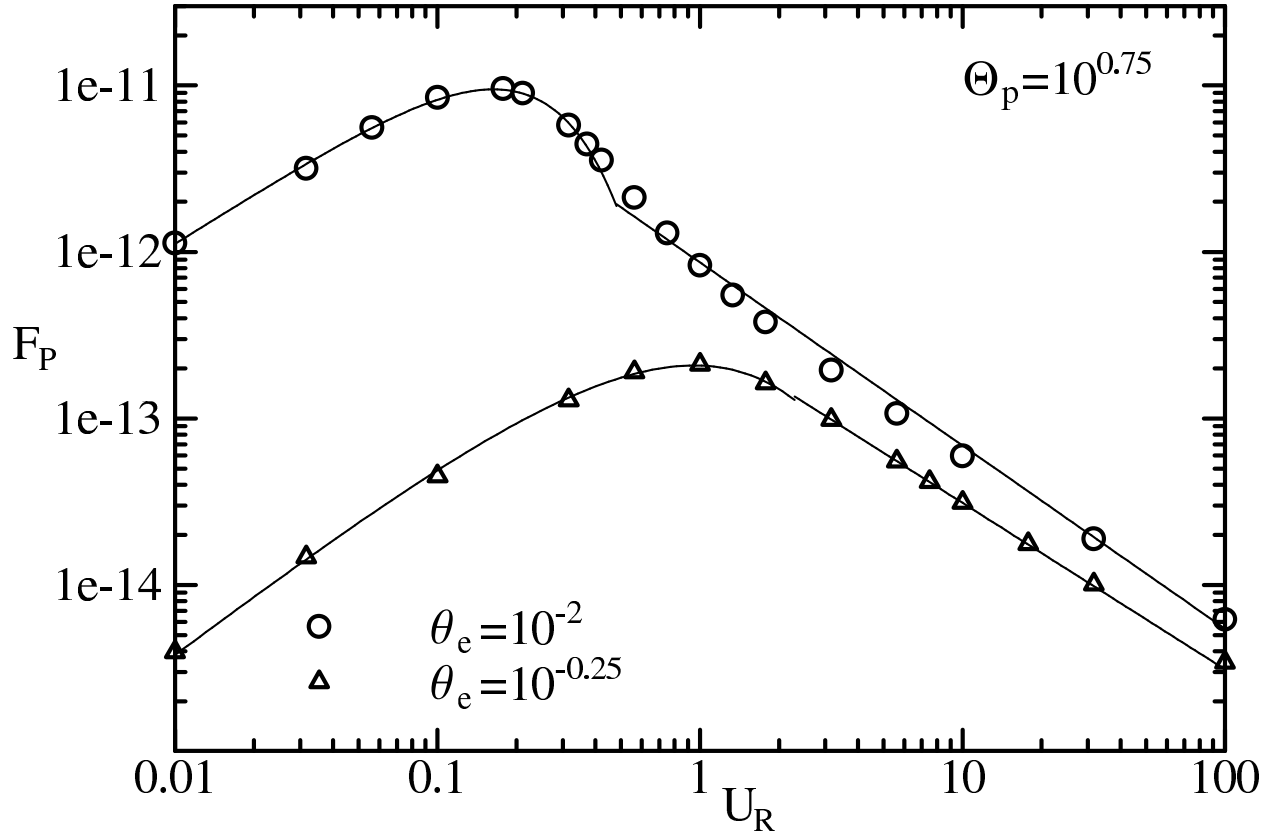


Fig. 5.— Two examples of the fitting functions for F_P of p-e interaction. Circles and triangles are our numerical results. Solid lines are the fitting functions we obtained (see equation (18) and Table 5).

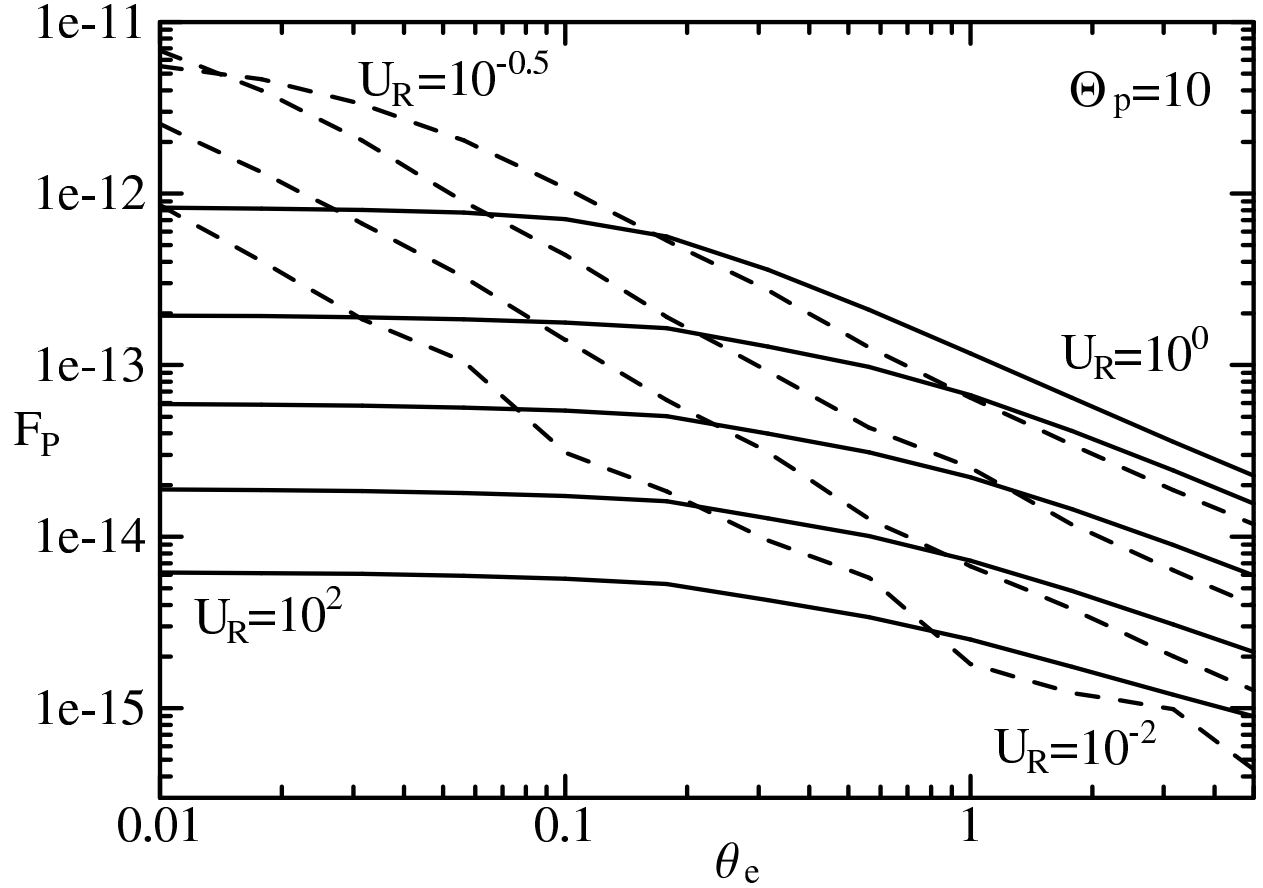


Fig. 6.— Same as Fig.4 but plotted vs. θ_e . Dashed lines are from $U_R = 10^{-2}$ to $10^{-0.5}$, and solid lines are from $U_R = 10^0$ to 10^2 at $10^{0.5}$ intervals in logarithmic scale.

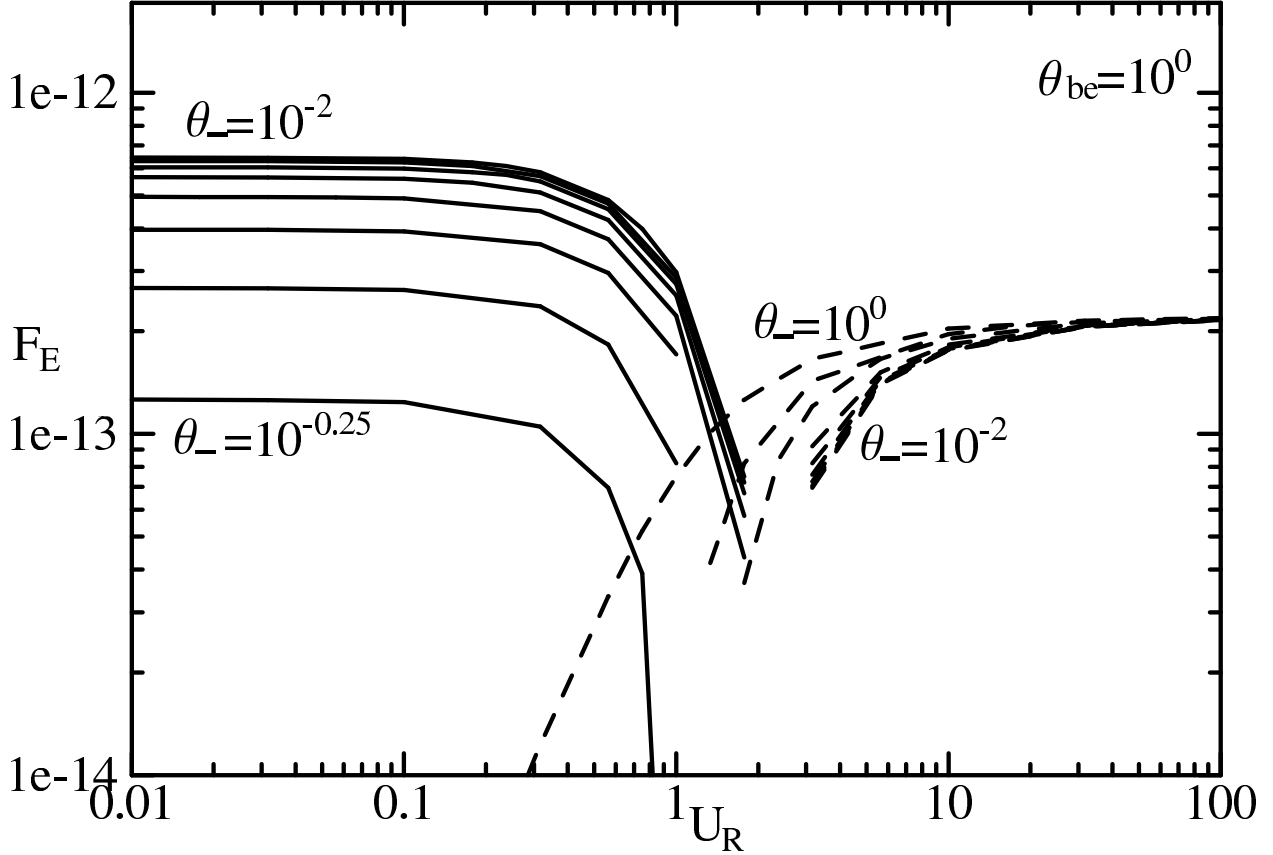


Fig. 7.— F_E of e^-e^- interaction for $\theta_{be} = 1$ in cgs unit. The temperatures of the outflowing electrons, θ_- , are from 10^{-2} to 10^0 at $10^{0.25}$ intervals in logarithmic scale. Dashed lines are $|F_E|$ for negative F_E .

From the figure we can see ET becomes zero at $U_R \sim$ a few, although it is difficult to determine the value of U_R , at which ET becomes zero, within our computational precision. As θ_- increases, $|F_E|$ also increases in cases of negative ET ($U_R \gtrsim 1$), while $|F_E|$ decreases for positive ET ($U_R \lesssim 1$).

When $U_R \gg \theta_{be}$, the thermal motion can be neglected. In this case, from equation (6), the energy loss of outflowing electrons in one collision $\langle \Delta E \rangle \sim U_R m_e c^2 \sin^2(\alpha/2)$. Since the mass of the colliding particle is the same, the Lorentz factor of electrons in the CM frame $\gamma \sim \gamma_{CM} \propto U_R^{1/2}$. The effective cross section $\sigma_{eff} \propto \gamma^{-2} \propto U_R^{-1}$ so that F_E becomes constant for $U_R \gg \theta_{be}$ as shown in Figure 7.

We fit our results by functions,

$$F_E = A_L \exp[-(U_R/U_L)^2], \quad (19)$$

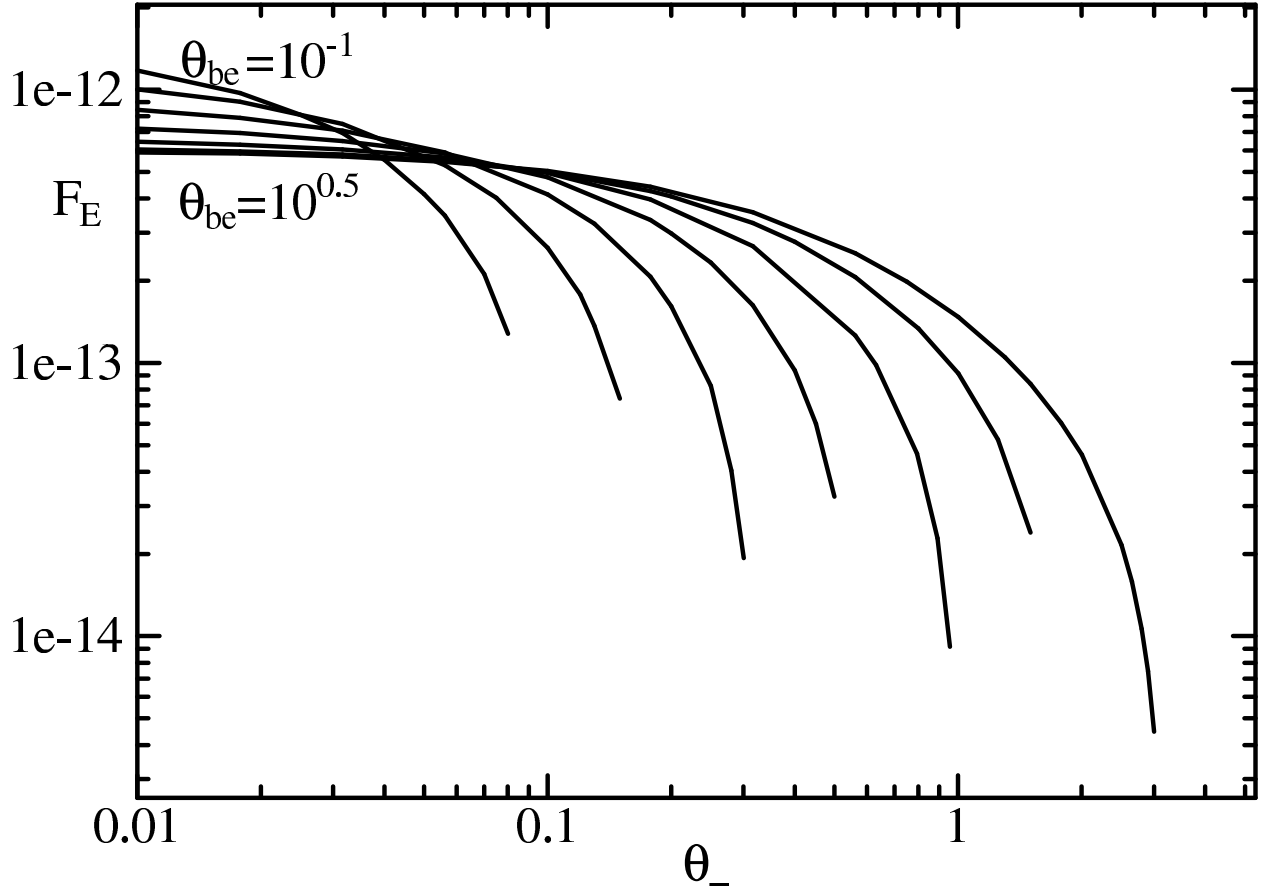


Fig. 8.— F_E of e^-e^- interaction for $U_R = 0$ in cgs unit. The temperatures of the background electrons, θ_{be} , are from 10^{-1} to $10^{0.5}$ at $10^{0.25}$ intervals in logarithmic scale.

for $U_R \lesssim 1$ and

$$F_E = -A_H \exp[-(U_R/U_H)^p], \quad (20)$$

for $U_R \gtrsim 1$. Fitting results are listed in Tables 11 and 12.

We tabulate the fitting parameters only for $\theta_{be} = 0.1$ and 1. However, as is shown in Figure 7, F_E is almost constant for $U_R \ll 1$. Thus, it is valuable to estimate F_E for $U_R = 0$ with a wide range of θ_{be} . Figure 8 shows the results, which are fitted by a function

$$F_E = A \exp[-(\theta_-/\theta_0)^p], \quad (21)$$

(see Table 13). Although the θ_{be} -dependence is hardly expressed by a simple formula, we can interpolate F_E from Table 13.

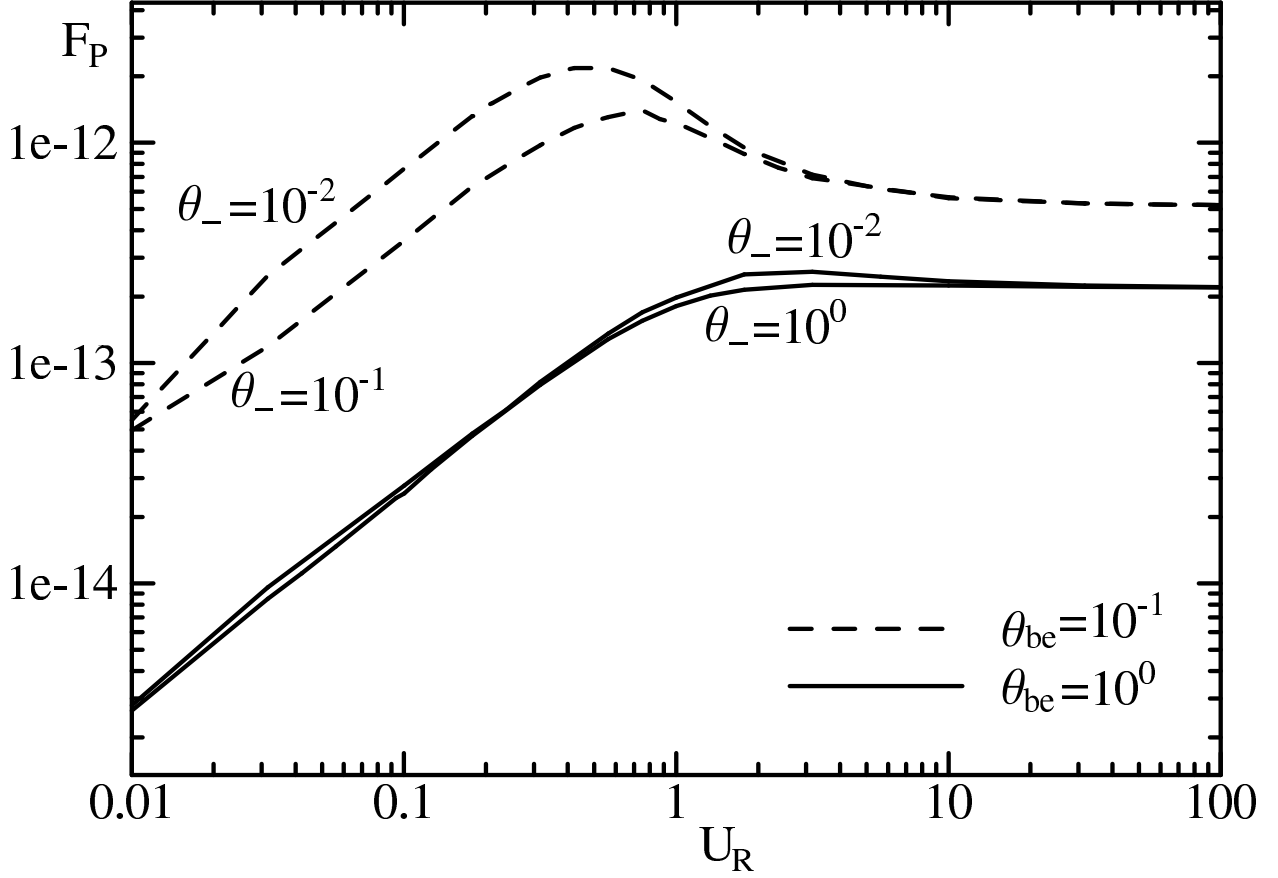


Fig. 9.— F_P of e^-e^- interaction in cgs unit.

3.4. MOMENTUM TRANSFER in e-e INTERACTION

As is the case with energy transfer, the momentum transfers for e^-e^- and e^-e^+ interactions are almost the same. The numerical results of F_P are plotted in Figure 9. For $\theta_{be} = 10^0$ the results are almost independent of the temperature of the outflowing electrons θ_- . Even for $\theta_{be} = 10^{-1}$, F_P decreases only by a factor of less than 2 with increasing $\theta_- = 10^{-2}$ to 10^{-1} . Figure 9 clearly shows the reduction of F_P due to increasing θ_{be} . As we have seen in the former cases, the growth of the average γ by rising θ_{be} results in the reduction of the cross section ($\sigma_{\text{eff}} \propto \gamma^{-2}\beta^{-4}$ for relativistic case). For $U_R \gg 1$, F_P is almost constant differently from the case of p-e interaction. This is because $\beta_{\text{CM}} \sim 1$ in e-e interaction and a resultant relation $\langle \Delta p \rangle \sim \langle \Delta E \rangle / c$. Therefore, our results show $F_P \simeq -F_E \propto U_R^0$ for $U_R \gg \theta_{be}$.

In contrast to p-e interaction, the cooling and heating properties of the two fluids in this case are the same. Therefore, if the flow velocity is non-relativistic, the two temperatures may be the same. Thus we calculate F_P mainly with $\theta_- = \theta_{be}$, as shown in Figure 10. Even

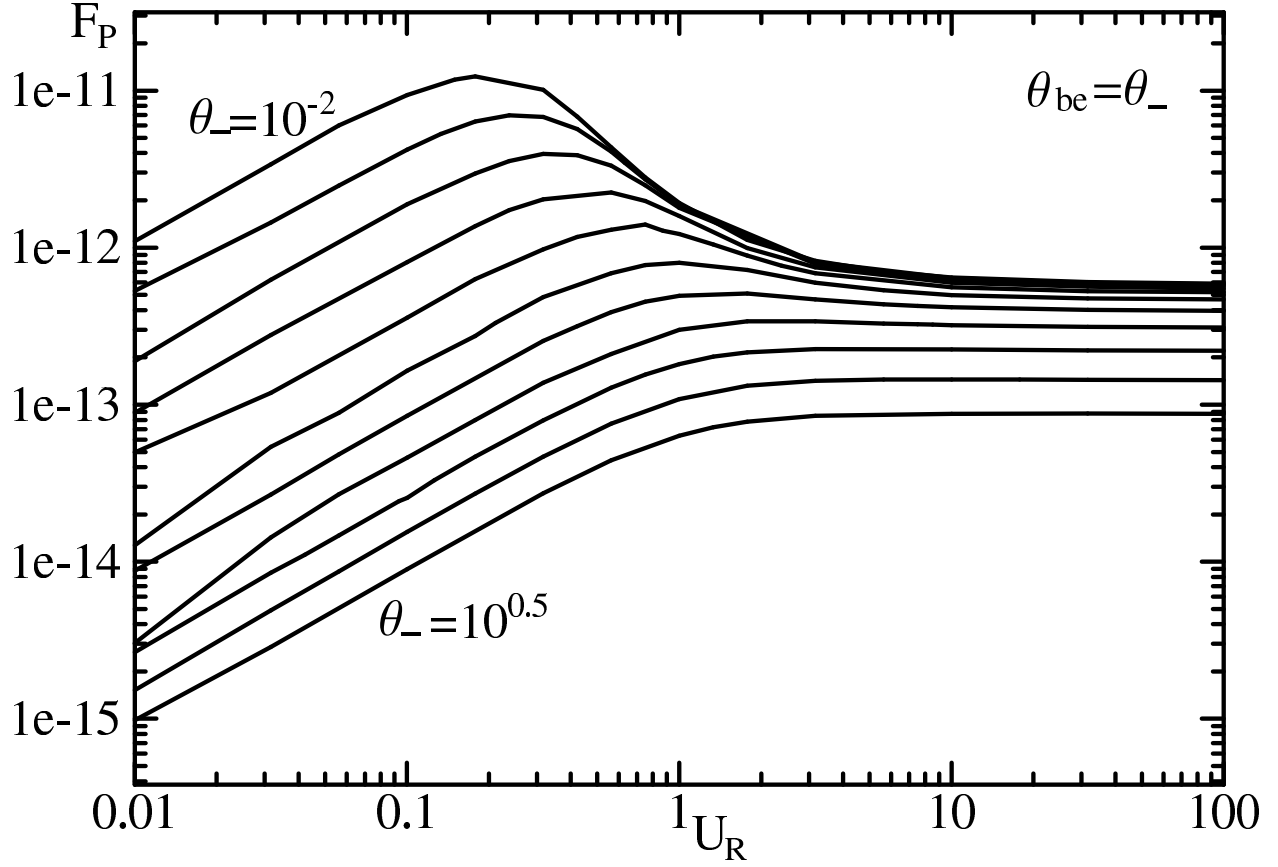


Fig. 10.— F_P of e^-e^- interaction for $\theta_{be} = \theta_-$ in cgs unit. The temperatures are from 10^{-2} to $10^{0.5}$ at $10^{0.25}$ intervals in logarithmic scale.

if the two temperatures are different, the correction is not so large as shown in Figure 9. We fit our results by functions;

$$F_P = \begin{cases} A_L \exp \left[- \left(\frac{U_R}{U_L} \right)^p \right] \left(\frac{U_R}{0.01} \right)^q, & \text{for } U_R < U_{th}, \\ A_H \exp \left[- \left(\frac{U_R}{U_H} \right)^r \right], & \text{for } U_R \geq U_{th}, \end{cases} \quad (22)$$

and results are summarized in Table 14. The symbol ∞ for U_H in this table means that F_P is constant as $F_P = A_H$ for $U_R \geq U_{th}$.

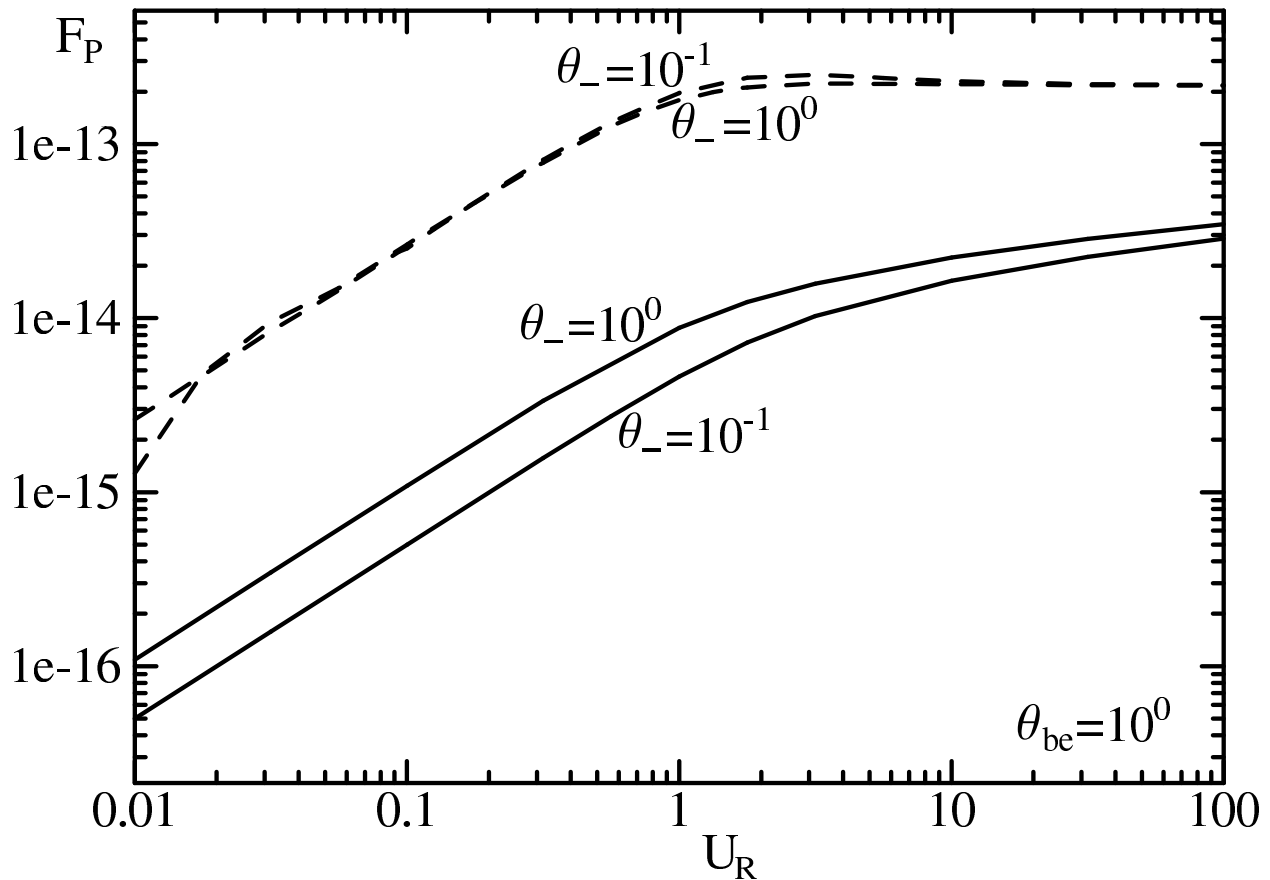


Fig. 11.— F_P of e^-e^+ interaction due to scattering (dashed) and pair-annihilation (solid) for $\theta_{be} = 10^0$ in cgs unit.

3.5. MOMENTUM TRANSFER in PAIR-ANNIHILATION

We shortly comment on the effect of pair-annihilation process here. The outflowing positrons may interact with the background electrons and turn into gamma-rays. This process decreases the momentum of the outflowing fluid, and it is not trivial whether we can neglect this momentum loss process or not. In Figure 11 we plot F_P of e^-e^+ due to pair-annihilation. As θ_- increases for $\theta_{be} = 10^0$, the momentum loss due to pair-annihilation increases, while that due to pair-scattering is almost constant. Even for $\theta_- = 10^0$, the momentum loss due to pair-annihilation is smaller than that due to pair-scattering by one order of magnitude.

For smaller values of $\theta_{be} < 10^0$, the contribution of pair-annihilation to F_P becomes much more negligible. Therefore, we can neglect the effect of pair-annihilation on the flow within precision we require.

4. SUMMARY

Motivated by electron-positron outflows from AGNs, we numerically calculate the energy and momentum transfer rates due to Coulomb scattering between two fluids with a relative velocity for plausible parameters in AGN models. Although several plasma effects, such as two-stream instability etc., may enhance the energy and momentum transfers, the effects of Coulomb scattering are the first to be taken into account. Our tables obtained from the numerical results are useful to simulate pair outflows from hot plasmas, or evaluate the interaction between AGN jets and the ambient medium. Especially, the momentum transfer rate is indispensable for such simulations. Using the results in this paper, a simulation in Asano & Takahara (2006) shows that the frictional force due to Coulomb scattering is comparable to radiative force for plausible parameter sets in AGN jet models. Therefore, we cannot neglect the effects of Coulomb scattering in such simulations.

We thank the anonymous referee for his useful comments. This work is partially supported by Scientific Research Grants (F.T. 14079205 and 16540215) from the Ministry of Education, Culture, Science and Technology of Japan.

REFERENCES

- Asano, K., & Takahara, F. 2006, submitted to ApJ
- Croston, J. H., Hardcastle, M. J., Harris, D. E., Belsole, E., Birkinshaw, M., & Worrall, D. M. 2005, ApJ, 626, 733
- Dermer, C. D. 1985, ApJ, 295, 28
- Hirotsu, K., Iguchi, S., Kimura, M., & Wajima, K. 1999, PASJ, 51, 263
- Hirotsu, K., Iguchi, S., Kimura, M., & Wajima, K. 2000, ApJ, 545, 100
- Hirotsu, K. 2005, ApJ, 619, 73
- Homan, D. C., & Wardle, J. F. C. 1999, AJ, 118, 1942
- Iwamoto, S., & Takahara, F. 2002, ApJ, 565, 163
- Iwamoto, S., & Takahara, F. 2004, ApJ, 601, 78
- Jauch, M. M. & Rohrlich, F., 1980. *The Theory of Photons and Electrons*, 2nd edn, Springer, Berlin.

- Kino, M., & Takahara, F. 2004, MNRAS, 349, 336
- Landau, L. D. & Lifshitz, E. M. 1975, *The classical theory of fields*, 4th edn, Pergamon Press, Oxford
- Li, H., & Liang, E. 1996, ApJ, 458, 514
- Liang, E., & Li, H. 1995, A&A, 298, L45
- Misra, R., & Melia, F. 1995, ApJ, 449, 813
- Ramaty, R., & Mészáros, P. 1981, ApJ, 250, 384
- Reynolds, C. S., Fabian, A. C., Celotti, A., & Rees, M. J. 1996, MNRAS, 283, 873
- Stepney, S. 1983, MNRAS, 202, 467
- Stepney, S. & Guilbert, P. W. 1983, MNRAS, 204, 1269
- Spitzer, L. 1956, *Physics of Fully Ionized Gases*, New York: Interscience Publishers, 1956,
- Takahara, F. 1994, in *Towards a Major Atmospheric Cerenkov Detector III*, ed. T.Kifune (Tokyo: Universal Academy), 131
- Takahara, F. 1997, in *Relativistic Jets in AGNs*, ed. M.Ostrowski, M.Sikora, G.Madejski, & M.Gegelman (Krakow: Jagiellonskieg Univ., Astron. Obs.), 253
- Wardle, J. F. C., Homan, D. C., Ojha, R., & Roberts, D. H. 1998, Nature, 395, 457
- Weaver, T. A. 1976, Phys. Rev. A, 13, 1563
- Yamasaki, T., Takahara, F. & Kusunose, M. 1999, ApJ, 523, L21

Table 1: Fitting parameters of F_E for p-e interaction, where $\Theta_p = 10^{0.75}$. See eq. (17).

| θ_e | A_L | U_0 | p | A_H | r | U_{th} |
|--------------|---------|-------|-----|---------|------|----------|
| 10^{-2} | 9.6e-13 | 0.166 | 2.0 | 3.0e-15 | -1.2 | 0.35 |
| $10^{-1.75}$ | 4.8e-13 | 0.209 | 2.0 | 3.1e-15 | -1.2 | 0.42 |
| $10^{-1.5}$ | 2.3e-13 | 0.275 | 2.0 | 3.1e-15 | -1.2 | 0.51 |
| $10^{-1.25}$ | 1.0e-13 | 0.369 | 2.0 | 3.1e-15 | -1.3 | 0.63 |
| 10^{-1} | 4.4e-14 | 0.508 | 2.0 | 3.5e-15 | -1.3 | 0.75 |
| $10^{-0.75}$ | 2.0e-14 | 0.673 | 2.0 | 4.2e-15 | -1.5 | 0.59 |
| $10^{-0.5}$ | 8.3e-15 | 1.008 | 1.5 | - | - | - |
| $10^{-0.25}$ | 3.6e-15 | 1.443 | 1.3 | - | - | - |
| $10^{0.0}$ | 1.7e-15 | 1.511 | 1.3 | - | - | - |

Table 2: Same as Table 1 but for $\Theta_p = 10$

| θ_e | A_L | U_0 | A_H | r | U_{th} |
|--------------|---------|-------|---------|------|----------|
| 10^{-2} | 1.4e-12 | 0.179 | 5.6e-15 | -1.2 | 0.37 |
| $10^{-1.75}$ | 7.3e-13 | 0.224 | 5.6e-15 | -1.2 | 0.44 |
| $10^{-1.5}$ | 3.7e-13 | 0.284 | 5.8e-15 | -1.2 | 0.52 |
| $10^{-1.25}$ | 1.7e-13 | 0.374 | 5.9e-15 | -1.2 | 0.63 |
| 10^{-1} | 7.7e-14 | 0.515 | 6.2e-15 | -1.2 | 0.76 |
| $10^{-0.75}$ | 3.5e-14 | 0.698 | 7.7e-15 | -1.4 | 0.69 |
| $10^{-0.5}$ | 1.5e-14 | 0.909 | 5.2e-15 | -1.4 | 0.76 |
| $10^{-0.25}$ | 7.0e-15 | 1.161 | 3.6e-15 | -1.4 | 1.01 |
| 10^0 | 3.2e-15 | 1.544 | 2.3e-15 | -1.4 | 1.31 |
| $10^{0.25}$ | 1.6e-15 | 1.359 | 9.8e-16 | -1.4 | 1.16 |
| $10^{0.5}$ | 7.1e-16 | 1.209 | - | - | - |

Table 3: Same as Table 1 but for $\Theta_p = 10^{1.5}$

| θ_e | A_L | U_0 | A_H | r | U_{th} |
|--------------|---------|-------|---------|------|----------|
| 10^{-2} | 1.8e-12 | 0.239 | 1.9e-14 | -1.2 | 0.45 |
| $10^{-1.75}$ | 1.3e-12 | 0.274 | 2.0e-14 | -1.2 | 0.50 |
| $10^{-1.5}$ | 7.7e-13 | 0.303 | 2.0e-14 | -1.2 | 0.51 |
| $10^{-1.25}$ | 4.1e-13 | 0.425 | 2.3e-14 | -1.2 | 0.66 |
| 10^{-1} | 2.1e-13 | 0.545 | 2.2e-14 | -1.2 | 0.75 |
| $10^{-0.75}$ | 9.9e-14 | 0.778 | 2.4e-14 | -1.3 | 0.87 |
| $10^{-0.5}$ | 4.7e-14 | 0.952 | 1.7e-14 | -1.3 | 0.79 |
| $10^{-0.25}$ | 2.2e-14 | 1.230 | 1.3e-14 | -1.3 | 1.04 |
| $10^{0.0}$ | 1.1e-14 | 1.479 | 6.9e-15 | -1.2 | 0.96 |
| $10^{0.25}$ | 5.6e-15 | 1.766 | 4.6e-15 | -1.3 | 1.19 |
| $10^{0.5}$ | 2.9e-15 | 1.783 | 2.5e-15 | -1.3 | 1.42 |

Table 4: Same as Table 1 but for $\Theta_p = 10^2$

| θ_e | A_L | U_0 | A_H | r | U_{th} |
|--------------|---------|-------|---------|------|----------|
| 10^{-2} | 1.6e-12 | 0.383 | 6.1e-14 | -1 | 0.65 |
| $10^{-1.75}$ | 1.4e-12 | 0.408 | 6.2e-14 | -1.1 | 0.66 |
| $10^{-1.5}$ | 1.1e-12 | 0.446 | 6.4e-14 | -1.1 | 0.69 |
| $10^{-1.25}$ | 7.3e-13 | 0.524 | 6.9e-14 | -1.2 | 0.74 |
| 10^{-1} | 4.4e-13 | 0.644 | 7.3e-14 | -1.2 | 0.80 |
| $10^{-0.75}$ | 2.5e-13 | 0.825 | 6.0e-14 | -1.2 | 0.96 |
| $10^{-0.5}$ | 1.3e-13 | 0.933 | 5.1e-14 | -1.2 | 0.75 |
| $10^{-0.25}$ | 6.4e-14 | 1.245 | 3.5e-14 | -1.1 | 0.95 |
| 10^0 | 3.3e-14 | 1.441 | 2.2e-14 | -1.1 | 1.10 |
| $10^{0.25}$ | 1.7e-14 | 1.630 | 1.3e-14 | -1.1 | 1.23 |
| $10^{0.5}$ | 9.4e-15 | 1.816 | 7.8e-15 | -1.1 | 1.37 |

Table 5: Same as Table 1 but for $\Theta_p = 10^{2.5}$

| θ_e | A_L | U_0 | p | A_H | r | U_{th} |
|--------------|---------|-------|-----|---------|------|----------|
| 10^{-2} | 1.1e-12 | 0.673 | 2.0 | 2.2e-13 | -1.1 | 0.79 |
| $10^{-1.75}$ | 1.0e-12 | 0.704 | 2.0 | 2.1e-13 | -1.1 | 0.83 |
| $10^{-1.5}$ | 9.4e-13 | 0.732 | 2.0 | 2.1e-13 | -1.1 | 0.83 |
| $10^{-1.25}$ | 8.0e-13 | 0.782 | 2.0 | 2.1e-13 | -1.1 | 0.84 |
| 10^{-1} | 6.2e-13 | 0.867 | 2.0 | 2.0e-13 | -1.1 | 0.86 |
| $10^{-0.75}$ | 4.3e-13 | 0.992 | 2.0 | 1.7e-13 | -1.1 | 0.87 |
| $10^{-0.5}$ | 2.7e-13 | 1.164 | 2.0 | 1.3e-13 | -1.1 | 1.05 |
| $10^{-0.25}$ | 1.5e-13 | 1.540 | 1.6 | 9.5e-14 | -1.1 | 1.36 |
| 10^0 | 8.5e-14 | 1.757 | 1.6 | 6.5e-14 | -1.1 | 1.45 |
| $10^{0.25}$ | 4.7e-14 | 1.924 | 1.6 | 4.1e-14 | -1.1 | 1.73 |
| $10^{0.5}$ | 2.6e-14 | 1.994 | 1.6 | 2.4e-14 | -1.1 | 1.68 |

Table 6: Fitting parameters of F_P for p-e interaction, where $\Theta_p = 10^{0.75}$. See eq. (18).

| θ_e | A_L | U_0 | p | q | A_H | r | U_{th} |
|--------------|---------|-------|-----|-----|---------|------|----------|
| 10^{-2} | 1.1e-12 | 0.214 | 1.5 | 1.0 | 8.7e-13 | -1.1 | 0.48 |
| $10^{-1.75}$ | 4.6e-13 | 0.255 | 1.5 | 1.1 | 7.8e-13 | -1.1 | 0.56 |
| $10^{-1.5}$ | 2.2e-13 | 0.322 | 1.5 | 1.1 | 7.8e-13 | -1.1 | 0.65 |
| $10^{-1.25}$ | 1.1e-13 | 0.502 | 1.5 | 1.0 | 7.8e-13 | -1.1 | 0.90 |
| 10^{-1} | 5.0e-14 | 0.631 | 1.5 | 1.0 | 5.6e-13 | -1.0 | 1.16 |
| $10^{-0.75}$ | 1.7e-14 | 0.700 | 1.3 | 1.1 | 5.6e-13 | -1.0 | 1.02 |
| $10^{-0.5}$ | 5.9e-15 | 0.713 | 1.0 | 1.2 | 4.1e-13 | -1.0 | 2.02 |
| $10^{-0.25}$ | 4.0e-15 | 0.572 | 0.8 | 1.2 | 3.1e-13 | -1.0 | 2.29 |
| $10^{0.0}$ | 2.3e-15 | 0.798 | 0.8 | 1.1 | 2.2e-13 | -1.0 | 2.70 |

Table 7: Same as Table 6 but for $\Theta_p = 10$

| θ_e | A_L | U_0 | p | q | A_H | r | U_{th} |
|--------------|---------|-------|-----|-----|---------|------|----------|
| 10^{-2} | 8.6e-13 | 0.237 | 1.5 | 1.0 | 1.1e-12 | -1.2 | 0.44 |
| $10^{-1.75}$ | 4.0e-13 | 0.257 | 1.5 | 1.1 | 8.1e-13 | -1.1 | 0.53 |
| $10^{-1.5}$ | 1.9e-13 | 0.341 | 1.5 | 1.1 | 7.9e-13 | -1.1 | 0.66 |
| $10^{-1.25}$ | 1.1e-13 | 0.488 | 1.5 | 1.0 | 7.5e-13 | -1.1 | 0.85 |
| 10^{-1} | 3.1e-14 | 0.512 | 1.5 | 1.2 | 6.8e-13 | -1.1 | 0.74 |
| $10^{-0.75}$ | 1.8e-14 | 0.914 | 1.5 | 1.0 | 5.6e-13 | -1.0 | 0.88 |
| $10^{-0.5}$ | 9.5e-15 | 1.074 | 1.5 | 1.0 | 4.1e-13 | -1.0 | 1.52 |
| $10^{-0.25}$ | 4.7e-15 | 1.195 | 1.2 | 1.0 | 3.0e-13 | -1.0 | 1.86 |
| $10^{0.0}$ | 1.8e-15 | 1.090 | 1.0 | 1.1 | 1.7e-13 | -0.9 | 2.75 |
| $10^{0.25}$ | 1.2e-15 | 1.418 | 1.0 | 1.0 | 1.2e-13 | -0.9 | 3.23 |
| $10^{0.5}$ | 9.9e-16 | 1.617 | 1.0 | 0.9 | 6.9e-14 | -0.9 | 3.44 |

Table 8: Same as Table 6 but for $\Theta_p = 10^{1.5}$

| θ_e | A_L | U_0 | p | q | A_H | r | U_{th} |
|--------------|---------|-------|-----|-----|---------|------|----------|
| 10^{-2} | 3.6e-13 | 0.329 | 1.5 | 1.0 | 7.7e-13 | -1.1 | 0.69 |
| $10^{-1.75}$ | 2.5e-13 | 0.359 | 1.5 | 1.0 | 7.6e-13 | -1.1 | 0.70 |
| $10^{-1.5}$ | 1.4e-13 | 0.359 | 1.5 | 1.1 | 7.5e-13 | -1.1 | 0.64 |
| $10^{-1.25}$ | 8.1e-14 | 0.538 | 1.5 | 1.0 | 7.2e-13 | -1.1 | 0.92 |
| 10^{-1} | 4.0e-14 | 0.676 | 1.5 | 1.0 | 6.6e-13 | -1.1 | 1.00 |
| $10^{-0.75}$ | 1.9e-14 | 0.866 | 1.5 | 1.0 | 5.3e-13 | -1.0 | 1.15 |
| $10^{-0.5}$ | 1.1e-14 | 1.271 | 1.8 | 0.9 | 4.0e-13 | -1.0 | 1.32 |
| $10^{-0.25}$ | 4.6e-15 | 1.187 | 1.2 | 1.0 | 2.9e-13 | -1.0 | 1.82 |
| $10^{0.0}$ | 2.0e-15 | 1.600 | 1.2 | 1.0 | 2.1e-13 | -1.0 | 3.24 |
| $10^{0.25}$ | 1.2e-15 | 1.560 | 1.2 | 1.0 | 1.1e-13 | -0.9 | 2.29 |
| $10^{0.5}$ | 5.5e-16 | 1.191 | 1.0 | 1.1 | 6.8e-14 | -0.9 | 2.39 |

Table 9: Same as Table 6 but for $\Theta_p = 10^2$

| θ_e | A_L | U_0 | p | q | A_H | r | U_{th} |
|--------------|---------|-------|-----|-----|---------|------|----------|
| 10^{-2} | 1.0e-13 | 0.478 | 1.5 | 1.0 | 7.2e-13 | -1.1 | 0.81 |
| $10^{-1.75}$ | 7.7e-14 | 0.527 | 1.5 | 1.0 | 7.1e-13 | -1.1 | 0.84 |
| $10^{-1.5}$ | 5.4e-14 | 0.463 | 1.5 | 1.1 | 6.7e-13 | -1.1 | 0.61 |
| $10^{-1.25}$ | 5.7e-14 | 0.697 | 1.5 | 0.9 | 5.3e-13 | -1.0 | 0.75 |
| 10^{-1} | 2.0e-14 | 0.677 | 1.5 | 1.1 | 5.7e-13 | -1.0 | 0.85 |
| $10^{-0.75}$ | 1.5e-14 | 0.876 | 1.3 | 1.0 | 4.9e-13 | -1.0 | 1.23 |
| $10^{-0.5}$ | 8.0e-15 | 1.047 | 1.3 | 1.0 | 3.6e-13 | -1.0 | 1.56 |
| $10^{-0.25}$ | 4.0e-15 | 1.229 | 1.3 | 1.0 | 2.6e-13 | -1.0 | 1.74 |
| $10^{0.0}$ | 2.3e-15 | 1.255 | 1.0 | 1.0 | 1.9e-13 | -1.0 | 2.51 |
| $10^{0.25}$ | 8.7e-16 | 1.139 | 1.0 | 1.1 | 9.5e-14 | -0.9 | 2.59 |
| $10^{0.5}$ | 6.7e-16 | 1.358 | 1.0 | 1.0 | 6.3e-14 | -0.9 | 2.63 |

Table 10: Same as Table 6 but for $\Theta_p = 10^{2.5}$

| θ_e | A_L | U_0 | p | q | A_H | r | U_{th} |
|--------------|---------|-------|-----|-----|---------|------|----------|
| 10^{-2} | 1.8e-14 | 0.783 | 1.5 | 1.0 | 4.6e-13 | -1.0 | 0.97 |
| $10^{-1.75}$ | 1.9e-14 | 1.008 | 2.0 | 0.9 | 4.5e-13 | -1.0 | 0.99 |
| $10^{-1.5}$ | 1.3e-14 | 0.925 | 2.0 | 1.0 | 4.3e-13 | -1.0 | 0.94 |
| $10^{-1.25}$ | 1.4e-14 | 1.102 | 2.5 | 0.9 | 4.0e-13 | -1.0 | 0.99 |
| 10^{-1} | 9.1e-15 | 1.042 | 1.5 | 1.0 | 4.0e-13 | -1.0 | 1.29 |
| $10^{-0.75}$ | 6.5e-15 | 1.178 | 1.5 | 1.0 | 3.6e-13 | -1.0 | 1.45 |
| $10^{-0.5}$ | 4.5e-15 | 1.218 | 1.5 | 1.0 | 2.8e-13 | -1.0 | 1.51 |
| $10^{-0.25}$ | 2.8e-15 | 1.298 | 1.1 | 1.0 | 2.2e-13 | -1.0 | 2.57 |
| $10^{0.0}$ | 1.6e-15 | 1.436 | 1.2 | 1.0 | 1.3e-13 | -0.9 | 2.11 |
| $10^{0.25}$ | 7.3e-16 | 1.124 | 1.0 | 1.1 | 8.5e-14 | -0.9 | 2.32 |
| $10^{0.5}$ | 4.7e-16 | 0.916 | 0.8 | 1.1 | 5.1e-14 | -0.9 | 2.89 |

Table 11: Fitting parameters of F_E for e–e interaction, where $\theta_{be} = 10^{-1}$. See eqs. (19) and (20).

| θ_- | A_L | U_L | A_H | U_H | p |
|--------------|---------|-------|---------|-------|-----|
| 10^{-2} | 1.2e-12 | 0.315 | 5.2e-13 | 0.5 | -3 |
| $10^{-1.75}$ | 9.7e-13 | 0.313 | 5.2e-13 | 0.5 | -3 |
| $10^{-1.5}$ | 6.8e-13 | 0.321 | 5.2e-13 | 0.5 | -3 |
| $10^{-1.25}$ | 3.4e-13 | 0.265 | 5.2e-13 | 0.5 | -3 |

Table 12: Same as Table 11 but for $\theta_{be} = 10^0$

| θ_- | A_L | U_L | A_H | U_H | p |
|--------------|---------|-------|---------|-------|------|
| 10^{-2} | 6.5e-13 | 1.117 | 2.2e-13 | 3.469 | -2 |
| $10^{-1.75}$ | 6.3e-13 | 1.124 | 2.2e-13 | 3.444 | -2 |
| $10^{-1.5}$ | 6.1e-13 | 1.123 | 2.2e-13 | 3.490 | -2 |
| $10^{-1.25}$ | 5.7e-13 | 1.112 | 2.2e-13 | 3.218 | -1.5 |
| 10^{-1} | 5.0e-13 | 1.104 | 2.2e-13 | 2.866 | -1.5 |
| $10^{-0.75}$ | 4.0e-13 | 1.076 | 2.2e-13 | 2.881 | -1.5 |
| $10^{-0.5}$ | 2.7e-13 | 0.915 | 2.2e-13 | 2.408 | -1.5 |
| $10^{-0.25}$ | 1.3e-13 | 0.679 | 2.2e-13 | 1.805 | -1.5 |

Table 13: Fitting parameters of F_E for e–e interaction for $U_R = 0$. See eq. (21).

| θ_{be} | A | θ_0 | p |
|---------------|---------|------------|-----|
| 10^{-1} | 1.2e-12 | 0.049 | 1.5 |
| $10^{-0.75}$ | 1.0e-12 | 0.080 | 1.4 |
| $10^{-0.5}$ | 8.5e-13 | 0.13 | 1.3 |
| $10^{-0.25}$ | 7.2e-13 | 0.22 | 1.3 |
| $10^{0.0}$ | 6.5e-13 | 0.35 | 1.2 |
| $10^{0.25}$ | 6.1e-13 | 0.52 | 1.0 |
| $10^{0.5}$ | 5.9e-13 | 0.7 | 1.0 |

Table 14: Fitting parameters of F_P for e-e interaction for $\theta_- = \theta_{\text{be}}$. See eq. (21).

| θ_e | A_L | U_L | p | q | A_H | U_H | r | U_{th} |
|--------------|---------|-------|------|-----|---------|----------|-------|-----------------|
| 10^{-2} | 1.1e-12 | 0.273 | 2.0 | 1.0 | 5.9e-13 | 1.111 | -0.85 | 0.36 |
| $10^{-1.75}$ | 5.3e-13 | 0.428 | 2.0 | 0.9 | 5.9e-13 | 1.093 | -0.9 | 0.55 |
| $10^{-1.5}$ | 1.9e-13 | 0.511 | 2.0 | 1.0 | 5.7e-13 | 1.023 | -1.0 | 1.16 |
| $10^{-1.25}$ | 8.9e-14 | 0.676 | 1.5 | 1.0 | 5.5e-13 | 1.059 | -1.0 | 0.89 |
| 10^{-1} | 5.0e-14 | 1.081 | 1.5 | 0.9 | 5.2e-13 | 0.888 | -1.0 | 1.38 |
| $10^{-0.75}$ | 1.3e-14 | 0.650 | 0.75 | 1.2 | 4.7e-13 | 0.762 | -1.0 | 2.33 |
| $10^{-0.5}$ | 8.8e-15 | 0.931 | 0.7 | 1.1 | 4.0e-13 | 0.525 | -1.0 | 3.13 |
| $10^{-0.25}$ | 3.0e-15 | 0.638 | 0.7 | 1.3 | 3.1e-13 | ∞ | - | 2.22 |
| $10^{0.0}$ | 2.7e-15 | 1.262 | 0.7 | 1.1 | 2.2e-13 | ∞ | - | 3.27 |
| $10^{0.25}$ | 1.5e-15 | 1.357 | 0.7 | 1.1 | 1.4e-13 | ∞ | - | 2.59 |
| $10^{0.5}$ | 9.8e-16 | 2.369 | 1.0 | 1.0 | 8.8e-14 | ∞ | - | 2.37 |

A. DIFFERENTIAL CROSS-SECTIONS FOR COULOMB SCATTERING

A.1. Electron-proton scattering: Rutherford cross-section

Differential cross section is given by

$$\frac{d\sigma}{d\Omega}(\beta, \alpha)_{\text{Rutherford}} = \frac{3\sigma_T}{32\pi\gamma^2\beta^4} \left(1 + \frac{2\gamma m_e}{m_p}\right) \frac{1}{\sin^4(\alpha/2)}, \quad (\text{A1})$$

(Stepney & Guilbert 1983), where β and γ is the velocity of electron and its Lorentz factor in the CM frame and σ_T is the Thomson cross section. From equations (6) and (7), we need to integrate $2\sin^2(\alpha/2)\frac{d\sigma}{d\Omega}$ over the scattering angles to obtain the energy and momentum transfer. Therefore, we define the effective cross-section as

$$\sigma_{\text{eff}} \equiv \int_{\alpha_{\text{min}}}^{\pi} (1 - \cos \alpha) \frac{d\sigma}{d\Omega} 2\pi \sin \alpha d\alpha. \quad (\text{A2})$$

Here α_{min} is the lower limit of scattering angle. Then we obtain

$$\sigma_{\text{eff,Rutherford}} = \frac{3\sigma_T}{2\gamma^2\beta^4} \left(1 + \frac{2\gamma m_e}{m_p}\right) \ln \Lambda, \quad (\text{A3})$$

where

$$\ln \Lambda \equiv \ln \left\{ \frac{1}{\sin(\alpha_{\text{min}}/2)} \right\}, \quad (\text{A4})$$

is the Coulomb logarithm and usually evaluated about $10 \sim 20$.

A.2. Electron-electron scattering: Møller cross-section

The differential cross-section of e^-e^- scattering (Jauch & Rohrlich 1980) is given by

$$\frac{d\sigma}{d\Omega}(\beta, \alpha)_{\text{Møller}} = \frac{3\sigma_T}{8\pi\gamma^2(\gamma^2 - 1)^2} \left[\frac{(2\gamma^2 - 1)^2}{\sin^4 \alpha} - \frac{2\gamma^4 - \gamma^2 - \frac{1}{4}}{\sin^2 \alpha} + \frac{(\gamma^2 - 1)^2}{4} \right]. \quad (\text{A5})$$

Since the particles are not identical, α is from α_{min} to $\pi/2$. In the same way as Rutherford scattering, we obtain the effective cross-section with $\Lambda \gg 1$ as

$$\sigma_{\text{eff,Møller}} = \frac{3\sigma_T}{16\gamma^6\beta^4} \left\{ (2\gamma^2 - 1)^2 [2 \ln \Lambda + 1] - 4 \left(2\gamma^4 - \gamma^2 - \frac{1}{4} \right) \ln 2 + \frac{\gamma^4\beta^4}{2} \right\}. \quad (\text{A6})$$

A.3. Electron-positron scattering: Bhabha cross-section

The differential cross-section of e^-e^+ scattering (Jauch & Rohrlich 1980) is given by

$$\begin{aligned} \frac{d\sigma}{d\Omega}(\beta, \alpha)_{\text{Bhabha}} = & \frac{3\sigma_T}{128\pi\gamma^2} \cdot \left\{ \frac{1}{[\gamma\beta \sin(\alpha/2)]^4} \left[1 + \left(2\gamma\beta \cos \frac{\alpha}{2} \right)^2 + 2(\gamma\beta)^4 \left(1 + \cos^4 \frac{\alpha}{2} \right) \right] \right. \\ & - \frac{1}{[\gamma^2\beta \sin(\alpha/2)]^2} \left[3 + 2 \left(2\gamma\beta \cos \frac{\alpha}{2} \right)^2 + \frac{1}{4} \left(2\gamma\beta \cos \frac{\alpha}{2} \right)^4 \right] \\ & \left. + \frac{1}{\gamma^4} [3 + 4(\gamma\beta)^2 + (\gamma\beta)^4(1 + \cos^2 \alpha)] \right\}. \end{aligned} \quad (\text{A7})$$

The effective cross-section is given by

$$\sigma_{\text{eff,Bhabha}} = \frac{3\sigma_T}{16} \left[\frac{2(2\gamma^2 - 1)^2}{\gamma^6\beta^4} \ln \Lambda - \frac{4\gamma^2 + 3}{\gamma^6\beta^2} - \frac{6\gamma^4 + 4\gamma^2 - 1}{2\gamma^6} - \frac{4\beta^2 - 2\beta^4}{3\gamma^2} \right]. \quad (\text{A8})$$